Advanced Steel Construction – Vol. 22 No. 1 (2026) 1–7
DOI:10.18057/IJASC.2026.22.1.1

HYSTERETIC BEHAVIOR OF ORTHOGONAL-INSTALLED DOUBLE CORRUGATED STEEL PLATE SHEAR WALL

Yan-Sheng Song [1], Zhuo-Yuan Jiang [1,*], Yu-Rong Dai [2] and Chun-Gang Wang [1]

[1] *School of Civil Engineering, Shenyang Jianzhu University, Shenyang 110168, China*
[2] *China Construction Fourth Bureau First construction Co., Ltd., Guangzhou 510000, China*
* *(Corresponding author: E-mail: jiangzy0922@163.com)*

ABSTRACT

To enhance the weak-axis performance of double corrugated steel plate shear walls (DCSPSWs), this study introduces an innovative orthogonal-installed double corrugated steel plate shear wall (OD-CSPSW). The proposed system comprises two orthogonally interlocked corrugated plates connected via through-bolts and integrated into a steel frame using fish-tail plate connections. A large-scale general-purpose finite element (FE) software, ABAQUS 6.14, was employed. Following validation against experimental benchmarks, 15 OD-CSPSW models were analyzed, and the effects of the corrugation angle and arrangement method on the hysteretic behavior of OD-CSPSWs were investigated. Additionally, two specimens of the co-directional DCSPSWs were designed as the control group. The results indicate that the OD-CSPSW demonstrates better hysteretic behavior compared to the co-directional DCSPSW. Specifically, the OD-CSPSW with a corrugation angle of 45° demonstrates the best overall stiffness and resistance to out-of-plane buckling, while also possessing a high energy dissipation capacity. According to the coverage method, the shear wall exhibits the highest initial stiffness when fully coverage, though its load-bearing capacity degrades more rapidly. For non-fully coverage, the energy dissipation capability of a vertically-centered shear wall outperforms a horizontally-centered one. It is recommended that when designing the OD-CSPSW, the corrugation angle should be set to 45° with full coverage, and if non-fully coverage is necessary, a vertically-centered arrangement should be selected.

ARTICLE HISTORY

Received: 30 December 2024
Revised: 3 June 2025
Accepted: 4 June 2025

KEYWORDS

Double steel corrugated plate wall;
Wave angles;
Coverage;
Hysteretic behavior;
FE analysis

1. Introduction

In recent years, the Corrugated Steel Plate Shear Wall (CSPSW) has emerged as a novel seismic-resistant structural component. The distinctive folded geometry of these systems has been proven effective in enhancing out-of-plane stability, improving elastic buckling strength, increasing energy dissipation capacity, and simplifying the construction process [1-3]. These advantages enable the CSPSW to play a crucial role in the structural stability and safety of high-rise buildings [4-8].

To evaluate the hysteretic performance of the CSPSW, Breman and Bruneau [9-11] conducted low-cycle reversed loading tests on shear walls made of flat steel plates and corrugated steel plates. Their comparative analysis of failure mechanisms and energy dissipation characteristics revealed that the CSPSW achieved better energy dissipation capacity and greater peak load resistance than the flat steel plate shear walls.

Furthermore, Ghodratian-Kashan et al. [12-15] focused on the performance evaluation and optimization design of corrugated steel plate shear walls including double-corrugated and single-corrugated types under cyclic loading. Through experiments and numerical simulations, they explored the influence of different connection designs and geometric parameters (e.g. plate thickness, aspect ratio, and corrugation direction) on the hysteretic behavior and seismic performance of the shear walls.

To mitigate local buckling instabilities prevalent in the conventional corrugated steel plate shear wall, researchers globally have proposed innovative configurations of double-corrugated steel plate shear wall (DC-SPSW). This design integrates two trapezoidal corrugated steel plates arranged in mirrored configurations along the horizontal/vertical axis, forming a composite system that capitalizes on the anisotropic properties of corrugated plates. When placed horizontally, the wall can avoid vertical loads through the "accordion effect" and mainly resist shear forces, whereas when placed vertically, it can effectively share vertical loads.

To address the weak-axis limitations of the DC-SPSW, this study proposes an orthogonal-installed Double Corrugated Steel Plate Shear Wall (OD-CSPSW). This configuration offers high bending stiffness in both the strong and weak axes, providing better deformation resistance and load-bearing capacity under both vertical and horizontal loads. Compared to single corrugated steel plate shear walls or traditional flat steel plate shear walls, the OD-CSPSW shows improvements in load-bearing capacity, energy dissipation, and hysteretic behavior.

Prior studies [17-26] have rarely investigated the application of orthogonally installed double corrugated steel plates in shear walls. To address this gap, this study designs 15 novel orthogonal double corrugated steel plate shear wall (OD-CSPSW) models, considering the distinctive characteristics of both horizontal and vertical placements of the corrugated steel plates. Building on prior studies [16], this paper further examines the influence of corrugation angle and arrangement method on the hysteretic behavior of the OD-CSPSW. Based on the findings from the parametric analysis, design recommendations are provided.

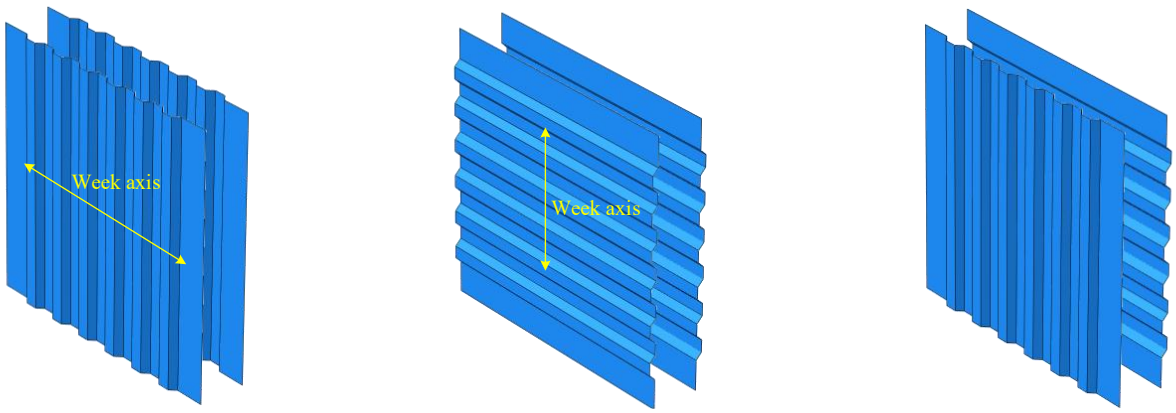

(a) VD-CSPSW (b) TD-CSPSW (c) OD-CSPSW

Fig. 1 Configuration of the insert steel plate

2. Configuration of the OD-CSPSW

The orthogonal double corrugated steel plate shear wall (OD-CSPSW) specimens investigated in this work, as illustrated in Fig. 1, comprise two orthogonally interlocked corrugated steel plates mechanically fastened at corrugation troughs using through-bolts and anchored to a two-story single-span steel frame via fish-tail plate connections. This unique orthogonal out-of-plane corrugated configuration achieves an effect similar to that of a flat steel plate shear wall with longitudinal and transverse stiffeners, enabling comparable shear resistance and seismic energy dissipation while eliminating the need for welded stiffeners. By replacing welded stiffeners with bolted corrugation interconnections, the OD-CSPSW achieves a reduction in weld volume, thereby mitigating weld-related failure risks inherent in conventional stiffened shear walls and simplifying on-site assembly processes. Compared to VD/TD-CSPSW, as shown in Fig. 1(a) and (b), OD-CSPSW combines the advantages of both, balancing load-bearing capabilities in two axial directions within the plane, and exhibits high potential for application.

3. FE models

3.1. Model calibration

A numerical analysis was conducted using the large-scale general-purpose FE software ABAQUS 6.14. To validate the numerical model, quasi-static test data of a two-story steel frame-steel plate shear wall structure from reference [16] were used for calibration. As shown in Fig. 2, the frame columns were selected as HW 200mm×200mm×8mm×12mm, the side beams as HN 250mm×200mm×12mm×14mm, the middle beams as HN 175mm×175mm×8mm×10mm, and the embedded steel plates were 2mm thick. The material of the frame was chosen as Q355B, and the embedded flat steel plates were made of Q235B, with a bilinear constitutive model.

Tie constraints were enforced between the top/bottom edges of the embedded steel plates and the outer frame. Similarly, the nodes at the left and right edges of the embedded steel plates were tied to the corresponding nodes at the contact surface in the outer frame. Both the outer frame and the embedded plates were modeled using shell elements (S4R) in the simulation, and an implicit dynamic analysis was performed. The column top was coupled at a point on the centroid line of the cross-section of the top beam of the frame, serving as the loading point.

The model was subjected to horizontal cyclic loading, with the loading protocol depicted in Fig. 3. Initially, load control was applied, with the following loading levels: 100 kN, 200 kN, 300 kN, 400 kN, 500 kN, 550 kN, 600 kN, and 650 kN, each level being cycled once. Afterward, displacement control was applied. The loading protocol comprised two phases: (1) eight stages (0.25%–2.0% drift) covering serviceability to ultimate limit states, aligned with the test program [16], and (2) six post-yield stages (2.5%–5.0% drift) to replicate the experimental program's planned loading-to-failure sequence. This approach ensured direct comparability of failure modes between FE simulations and physical tests.

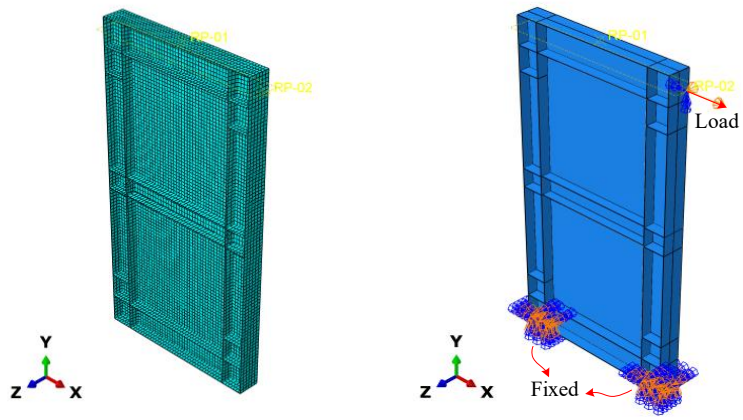

(a) Meshing (b) Boundary condition

Fig. 2 The establishment of FE model

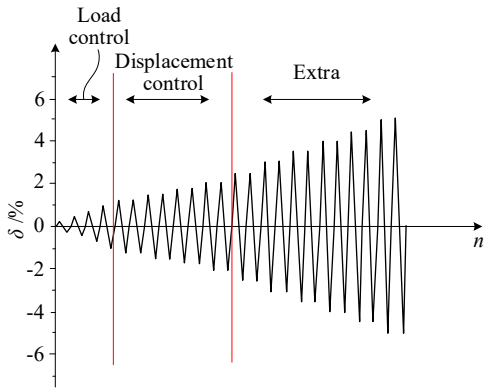

Fig. 3 Loading protocol

Fig. 4 shows a comparison between the FE and experimental hysteretic curves, skeleton curves, and stiffness degradation curves. It can be seen that the hysteretic curves obtained from numerical simulation and experiments exhibit a high degree of similarity in the shape of the hysteretic loops formed at each level. Both curves present a well-defined shape, displaying characteristics of both a spindle and a bow, with comparable enclosed areas within the loops. Based on the trend of the skeleton curve, it can be observed that the initial changes for both are consistent, with similar initial stiffness, a close plastic hinge point, and a similar development trend in the later stages. The numerical values are also close, with the largest error occurring at a displacement of 65 mm. At this point, the peak load in the experiment was 796.11 kN, while the finite element simulation value was 842.39 kN, showing a 5.8% overestimation. This discrepancy arises from the idealized boundary conditions in the FE model (e.g., perfect nodal ties and uniform material properties), which neglected experimental complexities such as additional constraints and localized imperfections that reduced the physical specimen's capacity. Additionally, the trend of the stiffness degradation curve in the finite element simulation is consistent with the experimental data, with the values being quite close. Therefore, the numerical analysis method used in this study accurately predicted the hysteretic behavior of the corrugated steel plate shear wall, and can be further applied to analyze the effects of corrugation angle and arrangement method on the hysteretic performance of corrugated steel plate shear walls.

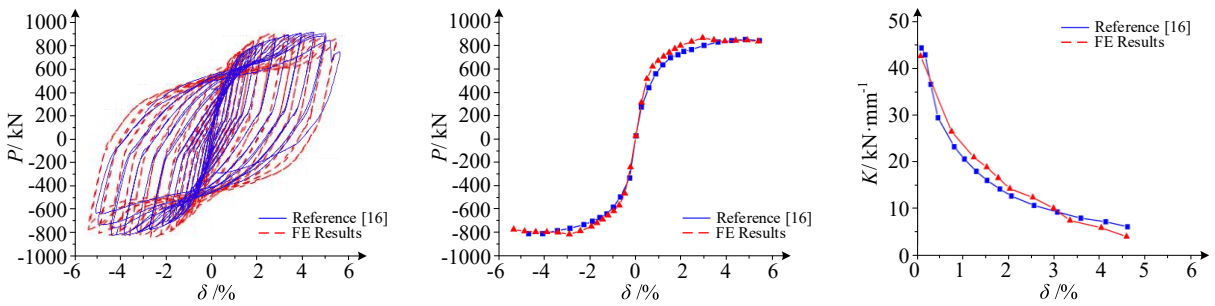

(a) Hysteretic curves (b) Skeleton curves (c) Stiffness degradation curves

Fig. 4 Comparison of hysteresis curves between test and FE results

3.2. FE models establish of the OD-CSPSW

To investigate the hysteretic behavior of orthogonal double corrugated steel plates, models for the transverse double corrugated steel plate shear wall (TD-CSPSW) and vertical double corrugated steel plate shear wall (VD-CSPSW) were designed. As shown in Fig. 5, to study the effect of the corrugation angle, three corrugation angles (30°, 45°, 90°) for the OD-CSPSW were considered based on their significant influence on the out-of-plane buckling resistance, shear stiffness, and energy dissipation capacity of the CSPSW [16,24]. Additionally, to explore material efficiency by reducing steel usage and enabling utility installations in non-fully covered regions, and to evaluate the impact of aspect ratio on seismic performance, five arrangement methods were considered: fully coverage (F), vertically-centered coverage (VC), horizontally-centered coverage (HC), vertically-split arrangement (VS), and horizontally-split coverage (HS). The latter four methods were non-fully coverage, with the aspect ratio of the embedded steel plates adjusted from 1.0 to 0.8. The coverage methods are shown in Fig. 6.

Based on the model validated through FE simulation, the arranged steel plates were replaced with the models mentioned above during assembly. The material constitutive relations for the steel plates, plate-frame interaction, boundary conditions, and loading conditions for the specimens were adjusted according to the control group, and the shear wall specimens were subjected to cyclic loading. A total of 17 cases as shown in Table 1 were analyzed for parametric studies, further investigating the hysteretic behavior of the orthogonal double corrugated steel plate shear walls.

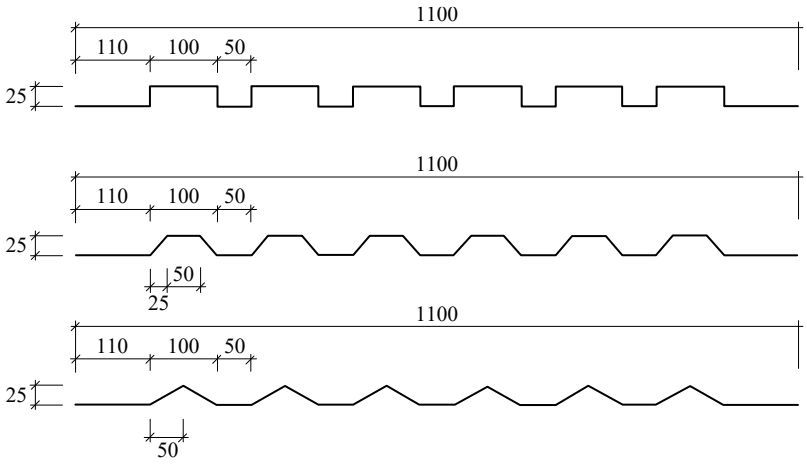

Fig. 5 Section dimensions of the steel plates

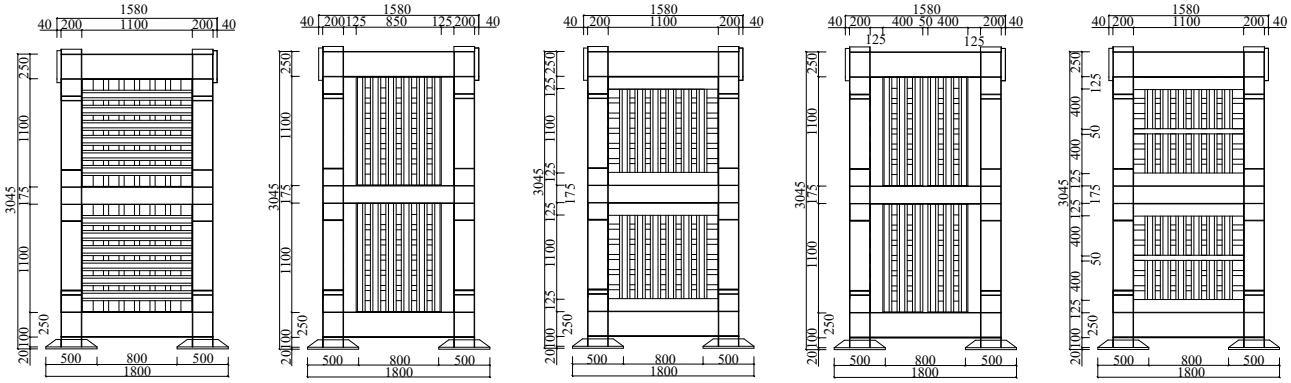

(a) F (b) VC (c) HC (d) VS (e) HS

Fig. 6 Arrangement modes and sizes of the steel plates (Unit: mm)

Table 1
Parameters of shear wall models

Models	Directions of corrugation	Corrugation angle	Coverage methods
OD-CSPSW-45-F	Orthogonal	45°	F
TD-CSPSW-45-F	Transverse	45°	F
VD-CSPSW-45-F	Vertical	45°	F
OD-CSPSW-90-F	Orthogonal	90°	F
OD-CSPSW-30-F	Orthogonal	30°	F
OD-CSPSW-90-VC	Orthogonal	90°	VC
OD-CSPSW-45-VC	Orthogonal	45°	VC
OD-CSPSW-30-VC	Orthogonal	30°	VC
OD-CSPSW-90-HC	Orthogonal	90°	HC
OD-CSPSW-45-HC	Orthogonal	45°	HC
OD-CSPSW-30-HC	Orthogonal	30°	HC
OD-CSPSW-90-VS	Orthogonal	90°	VS

OD-CSPSW-45-VS	Orthogonal	45°	VS
OD-CSPSW-30-VS	Orthogonal	30°	VS
OD-CSPSW-90-HS	Orthogonal	90°	HS
OD-CSPSW-45-HS	Orthogonal	45°	HS
OD-CSPSW-30-HS	Orthogonal	30°	HS

4. Analysis of FE results

4.1. Influence of the corrugation direction

Fig. 7 shows the stress distribution contours of the double corrugated steel plate shear walls (OD-CSPSW-45-F, TD-CSPSW-45-F, and VD-CSPSW-45-F) under failure conditions for different corrugation directions. Notably, transverse and vertical corrugation cases exhibit nearly identical failure modes. In both cases, a corrugated tensile band forms around the edges of the flat steel plate regions, with only the direction of the residual deformation differing. In contrast, the orthogonally configured OD-CSPSW-45-F demonstrates a fundamentally distinct failure mechanism: no diagonal tensile bands emerge, and residual deformations deviate from the conventional "X"-shaped pattern. Instead, the orthogonal corrugation interlocks promote uniform out-of-plane integrity, resulting in a concentric "O"-shaped bulge propagating radially from the plate center. This unique deformation mode correlates with a stress gradient where the annular "O"-shaped zone experiences lower von Mises stresses than its peripheral regions, suggesting enhanced stress redistribution capabilities through bidirectional corrugation synergy.

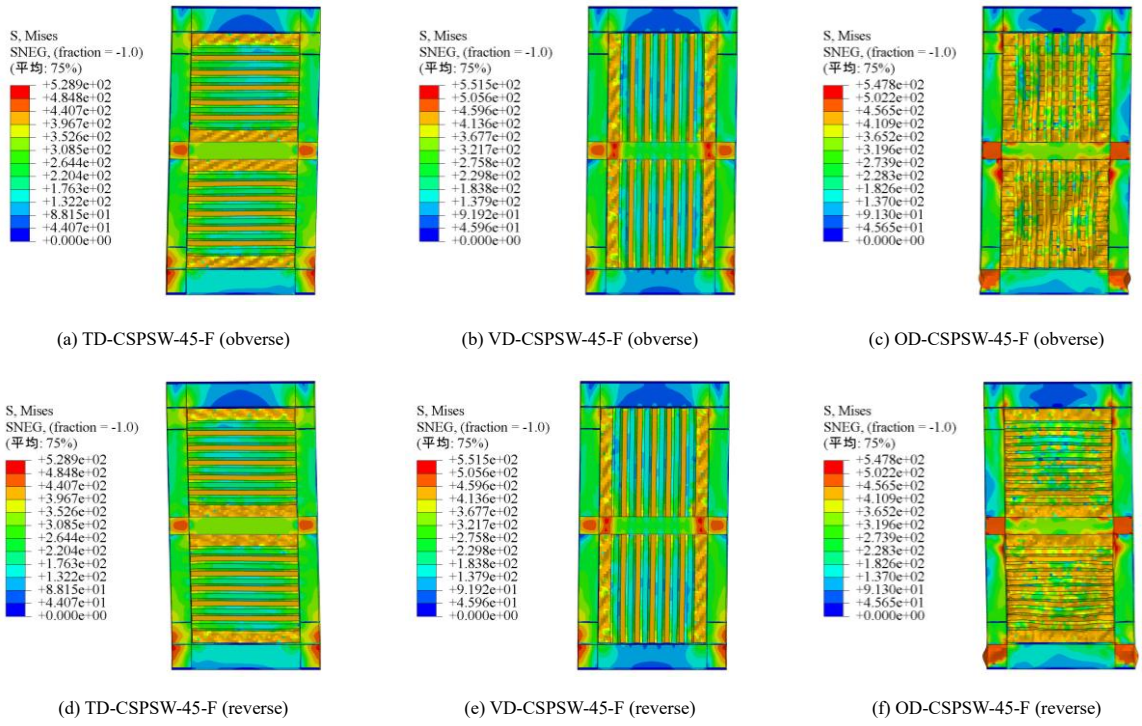

(a) TD-CSPSW-45-F (obverse) (b) VD-CSPSW-45-F (obverse) (c) OD-CSPSW-45-F (obverse)

(d) TD-CSPSW-45-F (reverse) (e) VD-CSPSW-45-F (reverse) (f) OD-CSPSW-45-F (reverse)

Fig. 7 Stress nephogram of failure state for example with different ripple directions (Unit: MPa)

Fig. 8 compares the hysteretic curves and cumulative energy dissipation capacities of double corrugated steel plate shear walls (OD-CSPSW-45-F, TD-CSPSW-45-F, and VD-CSPSW-45-F) under varying corrugation orientations. The results show that both VD-CSPSW-45-F and TD-CSPSW-45-F exhibit comparable cumulative energy dissipation, approximately 60,000 kN·m. In contrast, the cumulative energy dissipation of the OD-CSPSW-45-F model reaches nearly 220,000 kN·m, which is more than 3.5 times that of the VD and TD configurations. It can be concluded that the OD-CSPSW-45-F case exhibits the best energy dissipation capacity. This is due to the orthogonal installation of the embedded steel plates, which strengthens the original single-directional double corrugated steel plate shear wall's performance in the weak axis direction. As a result, the orthogonal double corrugated steel plate shear wall demonstrates high bending stiffness in both the strong and weak axis directions, meaning that the wall shows superior deformation resistance and load-bearing capacity when subjected to both vertical and horizontal loads.

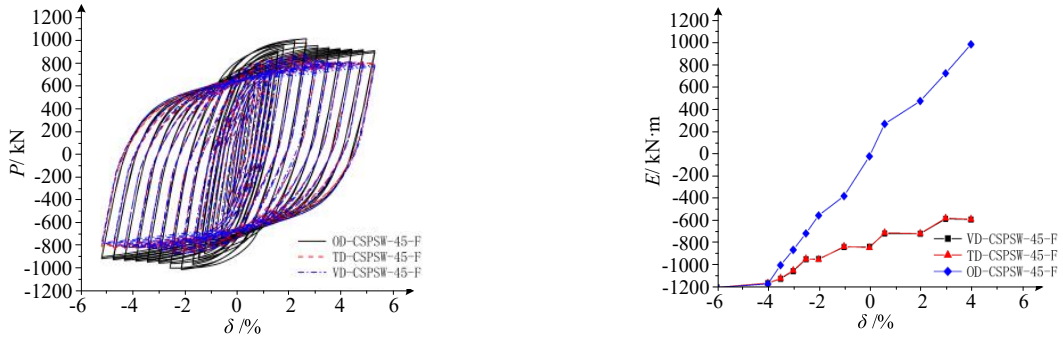

(a) Hysteretic curves (b) Energy dissipation curves

Fig. 8 Examples of hysteresis curves and energy dissipation capacity curves of different ripple directions

4.2. Influence of the corrugation angle

Fig. 9 depicts the stress distribution and failure mechanisms of orthogonal double corrugated steel plate shear walls (OD-CSPSW-90-F, OD-CSPSW-45-F, OD-CSPSW-30-F) under ultimate lateral drift (5%). For OD-CSPSW-90-F, the peak von Mises stress reached 539.20 MPa, accompanied by a maximum out-of-plane displacement of 96.07 mm. Similar to conventional shear walls, this configuration developed diagonal tension zones along the plate edges, with residual deformations forming a symmetrical "X" pattern. This is likely because the orthogonally distributed out-of-plane corrugations hinder the uniform development of the diagonal tensile bands, leading to a reduced "X" shaped stress distribution on the embedded steel plates.

In contrast, OD-CSPSW-30-F exhibited marginally higher peak stress (540.20 MPa) and greater out-of-plane displacement (106.30 mm). The embedded steel plates also display diagonal tensile bands and "X" shaped residual deformation. However, the "X" shape is less symmetrical than in the control group in [16] or the OD-CSPSW-90-F case. The "X" intersection of the upper steel plate is displaced downward, while the intersection of the lower steel plate shifts diagonally upwards to the right. Additionally, the stress at the column base and the node between the middle beam and the column is relatively high for the OD-CSPSW-30-F. For the OD-CSPSW-30-F case, the maximum stress is 540.20 MPa, and the maximum out-of-plane displacement is 106.30 mm. From the perspective of out-of-plane deformation, the OD-CSPSW-45-F exhibits the smallest deformation, followed by OD-CSPSW-90-F, and OD-CSPSW-30-F shows the largest out-of-plane deformation.

For the OD-CSPSW-45-F, the embedded steel plate's deformation predominantly localized along diagonal directions, manifesting as a diagonal wave-shaped buckling pattern. This contrasts with the orthogonally staggered 90° corrugations, whose geometric configuration mimics the mechanical function of bidirectional stiffeners (longitudinal and transverse). By restricting lateral displacement through corrugation interlocking, this orthogonal arrangement suppresses out-of-plane buckling instabilities, achieving a reduction in peak out-of-plane displacement compared to conventional stiffened shear walls. Consequently, the resultant wave-shaped deformations in OD-CSPSW-90-F are less pronounced and more uniformly distributed than those observed in non-orthogonal configurations.

The OD-CSPSW-90-F case shows an "O"-shaped out-of-plane bulge at the center of the embedded steel plate, and the bulge and its range for the lower steel plate are greater than those of the upper steel plate. The OD-CSPSW-30-F case also concentrates out-of-plane deformation along the diagonal, forming an asymmetric "X"-shaped bulge, and the intersection points of the "X" shape exhibit sharp out-of-plane deformation. This indicates that the triangular corrugated cross-section is disadvantageous for preventing out-of-plane buckling of the embedded steel plates.

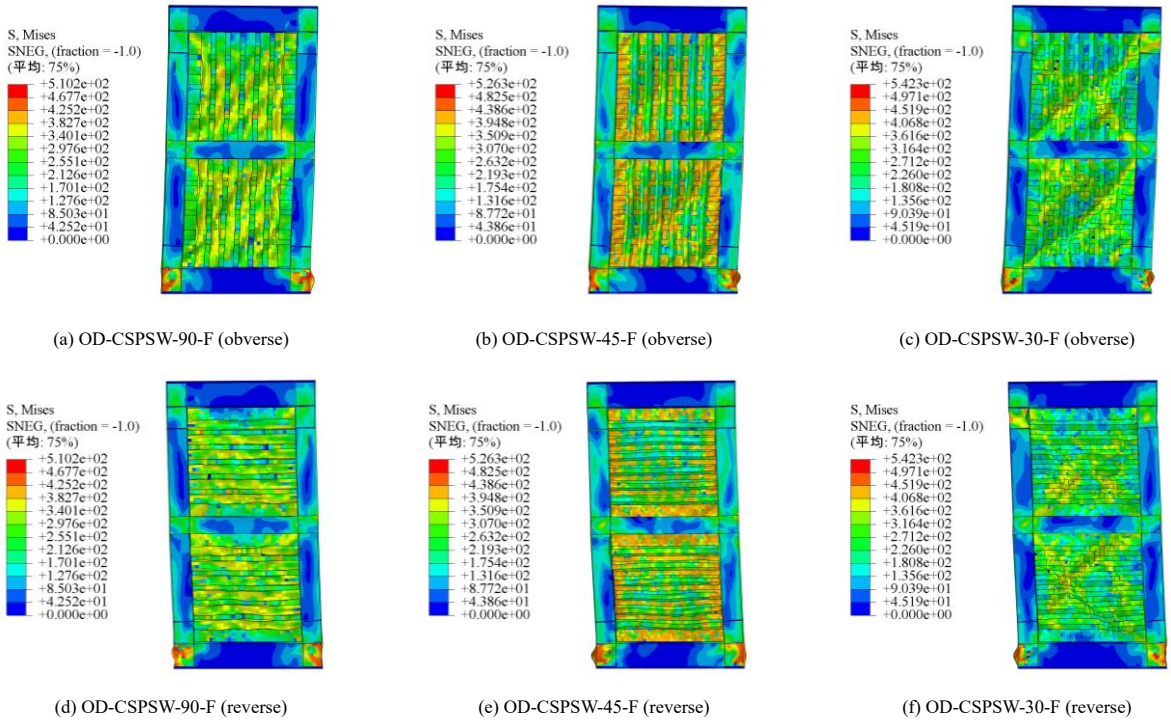

(a) OD-CSPSW-90-F (obverse) (b) OD-CSPSW-45-F (obverse) (c) OD-CSPSW-30-F (obverse)

(d) OD-CSPSW-90-F (reverse) (e) OD-CSPSW-45-F (reverse) (f) OD-CSPSW-30-F (reverse)

Fig. 9 The stress cloud diagram of the failure state of the example with different twist angles (Unit: MPa)

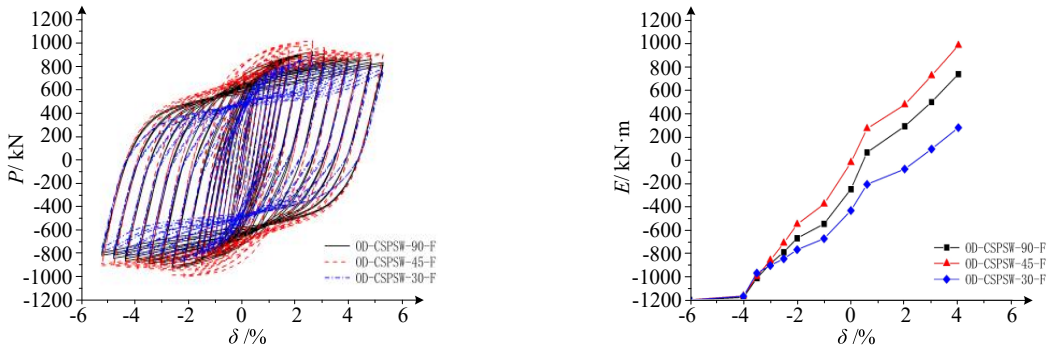

(a) Hysteretic curves (b) Energy dissipation curves

Fig. 10 Examples of hysteresis curve and energy dissipation capacity curve of different bending angles

Under cyclic loading, the lateral load-displacement hysteretic curves of the models are shown in Fig. 10. All models with different corrugation angles demonstrate stable hysteretic performance. The comparison reveals that the hysteretic curves for OD-CSPSW-90-F and OD-CSPSW-45-F are fully enclosed, with OD-CSPSW-45-F displaying the highest loop completeness. In contrast, the hysteretic curves for OD-CSPSW-30-F exhibit significant pinching. Therefore, the energy dissipation capacity ranks as OD-CSPSW-45-F > OD-CSPSW-90-F > OD-CSPSW-30-F, despite the apparent discrepancy in

cumulative energy values (1938.2, 2183.6, and 1478.8 kN·m, respectively), which may require further validation. The equivalent viscous damping coefficients are 0.36, 0.38, and 0.30, respectively.

Combining the analysis of the failure states, it can be concluded that the OD-CSPSW-45-F model benefits from the orthogonal superposition of 45° corrugated steel plates, which enhances its out-of-plane integrity and improves its seismic performance. In contrast, the OD-CSPSW-90-F and OD-CSPSW-30-F models exhibit gradual post-peak strength degradation despite inelastic buckling of the infill plates. This behavior stems from the sustained load-bearing capacity of the diagonal tension fields formed after yielding: even as partial unloading occurs due to out-of-plane deformations, stress redistribution through these diagonal tensile mechanisms enables progressive failure rather than abrupt collapse. The OD-CSPSW-45-F's absence of such tension bands further underscores its distinct failure mechanism, where bidirectional corrugation synergy replaces localized tension fields with uniform stress dispersion.

4.3. Influence of the coverage method

Under cyclic loading with VC as shown in Fig. 11(a), the lateral load-lateral displacement hysteretic curves for the specimens OD-CSPSW-45-VC, OD-CSPSW-30-VC, and OD-CSPSW-90-VC exhibit good hysteretic performance, with all curves showing a full and closed shape. Evaluation of loop fullness and peak load magnitudes revealed marginally superior energy dissipation capacities in OD-CSPSW-45-VC and OD-CSPSW-30-VC compared to OD-CSPSW-90-VC. Distinct failure modes emerged across configurations: OD-CSPSW-90-VC and OD-CSPSW-30-VC developed prominent "H"-shaped residual deformations with incomplete annular out-of-plane buckling patterns, particularly pronounced in OD-CSPSW-30-VC where buckling localized eccentrically (peak displacement = 106.30 mm). In contrast, OD-CSPSW-45-VC exhibited preferential bidirectional outward flexural buckling along diagonal axes. Mechanistically, asymmetric outward bending in OD-CSPSW-45-VC promoted distributed plasticity and delayed strain localization, while symmetric "H"-shaped or eccentric annular buckling in OD-CSPSW-90/30-VC accelerated localized yielding. This asymmetric deformation mode enhanced energy dissipation through controlled plastic hinge formation, establishing the performance hierarchy: OD-CSPSW-45-VC surpassed OD-CSPSW-30-VC, which outperformed OD-CSPSW-90-VC in cumulative energy dissipation efficiency.

Under the condition of HC as described in Fig. 11(b), the specimens OD-CSPSW-45-HC, OD-CSPSW-30-HC, and OD-CSPSW-90-HC exhibit good hysteretic curves during lateral load-displacement cyclic loading, with full and similar shapes. Preliminary analysis indicates that OD-CSPSW-45-HC and OD-CSPSW-30-HC perform slightly better than OD-CSPSW-90-HC in energy dissipation. Further observation of the failure modes reveals that all specimens show vertical outward buckling of the embedded steel plates, and the back of the OD-CSPSW-90-HC specimen exhibits significant "H"-shaped residual deformation and localized circular out-of-plane bulging in the upper steel plates. It can be inferred that the "H"-shaped residual deformation and bulging phenomena are detrimental to energy dissipation, whereas the vertical outward buckling is an early manifestation of circular bulging. Overall, the corrugation angle has a minimal impact on the hysteretic curve in arrangement method 2, though further parameter analyses may reveal more details.

Under the condition of VS as described in Fig. 11(c), the hysteretic curve performance of specimens OD-CSPSW-90-VS, OD-CSPSW-45-VS, and OD-CSPSW-30-VS shows minimal difference. The hysteretic curves of the three groups maintain high fullness and exhibit similar deformation trends. Although the effect of the corrugation angle on the hysteretic performance is not very significant, the lower steel plates of OD-CSPSW-30-VS show notable outward buckling. Analysis of the out-of-plane deformation level reveals the order of deformation severity as OD-CSPSW-90-VS, OD-CSPSW-45-VS, and OD-CSPSW-30-VS in descending order of severity.

Under the condition of HS as shown in Fig. 11(d), the specimens OD-CSPSW-45-HS, OD-CSPSW-30-HS, and OD-CSPSW-90-HS also demonstrate full hysteretic curves, with similar hysteretic performance and consistent curve shapes. In terms of energy dissipation, OD-CSPSW-45-HS and OD-CSPSW-30-HS perform slightly better than OD-CSPSW-90-HS, although the differences are not significant. Observation of the failure modes reveals that OD-CSPSW-45-HS and OD-CSPSW-30-HS show more pronounced outward buckling in the lower embedded steel plates. It can be inferred that under arrangement method 4, the energy dissipation performance ranks from high to low as follows: OD-CSPSW-45-HS, OD-CSPSW-30-HS, and OD-CSPSW-90-HS.

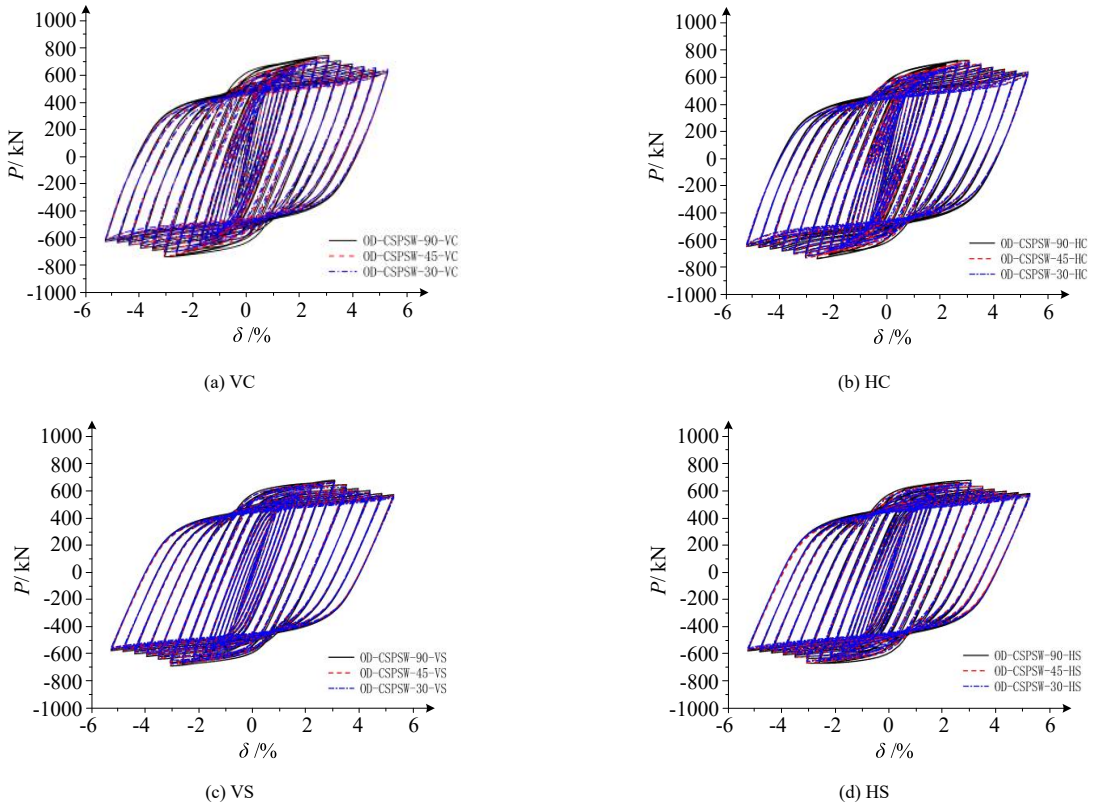

(a) VC (b) HC

(c) VS (d) HS

Fig. 11 Hysteresis curves under different arrangements

5. Conclusions

This study employs the finite element software ABAQUS to simulate the cyclic loading of 17 DCSPSW and investigates the effects of corrugation direction, corrugation angle, and arrangement method on their mechanical performance. The following conclusions were drawn:

(1) The unidirectional double corrugated steel plate shear wall and the orthogonal double corrugated steel plate shear wall exhibit significant differences in lateral resistance performance. While the unidirectional double corrugated steel plate shear wall improved the lateral stiffness of the embedded

steel plate in the early stages, its load-bearing capacity decreased due to severe out-of-plane deformation in the later stages. In contrast, the orthogonal double corrugated steel plate shear wall demonstrates clear advantages in both ultimate load-bearing capacity and energy dissipation capacity. Its structural design more effectively delays out-of-plane deformation, thereby enhancing overall stability and energy dissipation.

(2) The initial lateral stiffness of the orthogonal double corrugated steel plate shear wall decreases sequentially as the corrugation angle increases from 30° to 90°. When factors such as lateral stiffness, out-of-plane buckling resistance, and energy dissipation capacity are considered, the steel plate with a 45° corrugation angle offers a more balanced overall performance. It not only exhibits good initial lateral stiffness but also demonstrates strong resistance to out-of-plane buckling. In terms of energy dissipation capacity, the 45° corrugated steel plate outperforms other corrugation angles, with its hysteretic curve being full and energy dissipation being uniform, showing stable hysteretic performance.

(3) The hysteretic performance of the orthogonal double corrugated steel plate shear wall is also significantly influenced by the arrangement method and the area of the embedded steel plates. Orthogonal double corrugated steel plates with larger areas exhibit stronger energy dissipation capacity, higher initial stiffness, and greater peak load. In the fully-covered arrangement, the initial stiffness is the highest, but the load-bearing capacity degrades more rapidly. In non-fully-covered cases, the energy dissipation capacity of the vertically-centered arrangement is better than that of the split arrangement, while the horizontally-centered arrangement shows the opposite trend. Overall, the energy dissipation of the vertically-centered single plates is better than that of the horizontally-centered arrangement, but for split arrangements, the energy dissipation of the horizontally-centered embedded steel plates is better than that of the vertically-centered ones.

(4) The orthogonal double corrugated steel plate shear wall demonstrates superior energy dissipation capacity and load-bearing stability under various conditions of corrugation angle, arrangement method, and embedded steel plate area. The corrugation angle plays a key role in improving stiffness and ductility, with the 45° corrugation angle performing best in terms of overall integrity and anti-buckling capability. Furthermore, the rational configuration of the arrangement method and plate area can significantly enhance the mechanical performance. By optimizing these factors comprehensively, excellent hysteretic performance and stable lateral stiffness of the steel plate shear walls can be achieved in practical applications.

While the OD-CSPSW with 45° corrugation and full coverage demonstrates superior performance, its real-world implementation faces challenges. The orthogonal interlocking configuration demands precise fabrication and alignment during installation, potentially increasing labor costs. Additionally, full coverage requires more material than non-fully covered arrangements, though this trade-off may be justified in seismically active regions due to enhanced energy dissipation. To mitigate these challenges, prefabricated modular panels and standardized bolted connections (e.g., pre-assembled fish-tail plates) are recommended to reduce on-site complexity. Future studies should further explore cost-benefit analyses and lightweight optimization strategies for broader applicability.

Declaration of competing interest

The authors declare that they have no known competing financial interests or personal relationships that could have appeared to influence the work reported in this paper.

Acknowledgments

This study was financially supported by the China Construction Shares Technology Research and Development Project (CSCEC-2010-Z-01-02, CSCEC-2010-C-05).

References

[1] Zand SMD, Kalatjari V, Attari NK A. Cyclic performance of new steel plate shear wall reinforced by trapezoidal corrugated plate [J]. Journal of Architectural Journal,2017,35(1):11-11 Journal of Civil Engineering, Institute of Technology,2023.

[2] Bahrebar Milad, Lim James B.P., Clifton George Charles. Response assessment and prediction of low yield point steel plate shear walls with curved corrugated web plates and reduced beam sections[J]. Structures,2020,28.

[3] Bahrebar Milad, Kabir M Z, Zirakian T, et al. Structural Performance Assessment of Trapezoidally-Corrugated and Centrally-Perforated Steel Plate Shear Walls[J]. Journal of Constructional Steel Research, 2016(122):584-594.

[4] Jin H.J., Sun F.F., Li G.Q.. Simplified inelastic global buckling theory of non-buckling corrugated steel shear walls for seismic energy dissipation[J]. Thin-Walled Structures,2021,159.

[5] Fadhil H, Ibrahim I, Mahmood M. Effect of Corrugation Angle and Direction on the Performance of Corrugated Steel Plate Shear Walls[J]. Civil Engineering Journal, 2018,4(11):2667-2679.

[6] Yu C, Yu G. Experimental Investigation of Cold-Formed Steel Framed Shear Wall Using Corrugated Steel Sheathing with Circular Holes[J]. Journal of Structural Engineering, 2016, 142(12):04016126:8.

[7] Rajeev A, Jacob B, Muhamed S. Evaluation and Comparison of Behavior of Trapezoidally Corrugated Steel Plate Shear Walls[J]. International Research Journal of Engineering and Technology, 2016,3(9):318-327.

[8] Dou C, Jiang Z, Pi Y, et al. Elastic Shear Buckling of Sinusoidally Corrugated Steel Plate Shear Wall[J]. Engineering Structures, 2016(121):136-146.

[9] Hosseinzadeh L, Emami F, Mofid M. Experimental study on Performance of corrugated steel shear walls under Different trapezoidal plate Angles [J]. High-rise and Special Building Structure Design,2017,26(17):e1390.

[10] J. W. Berman, M. Bruneau. Experimental Invetigation of Light-Gauge Steel Plate Shear Walls[J]. Journal of Structural Engineering, 2005, 131(2):259-267.

[11] J. W. Berman, M. Bruneau. Experimental Investigation of Light-Gauge Steel Plate Shear Walls for The Seismic Retrofit of Building[R]. Tech. Rep. No. Mceer-03-0001:Multidisciplinary center for earthquake engineering research, Univ. at Buffalo, N. Y., 2003.

[12] Ghodratian-Kashan, SM,Maleki S. Experimental investigation of double corrugated steel plate shear walls [J]. Journal of Architectural Journal,2017,35(1):11-11 .

[13] Ghodratian-Kashan, SM,Maleki S. Experimental and Numerical Study of Beam-Only-Connected Corrugated Steel Plate Shear Walls[J]. Journal of Earthquake Engineering,2023:1-23.

[14] Ghodratian-Kashan, SM,Maleki S. Numerical study of Double corrugated steel plate shear Wall [J]. Journal of Civil Engineering and Construction,2021,10(1):44-58.

[15] Ghodratian-Kashan, SM,Maleki S. Experimental study on Double corrugated steel plate shear wall [J]. Journal of Building Steel Research,2022,190:107138.

[16] Qiuhong Zhao, Jing Qiu, Bochao Hao, et al. Lateral resistance of vertical corrugated steel plate shear walls with Two Sides Connected [J]. Journal of Tianjin University (Natural Science and Engineering Technology),2019,52(S2):46-53.

[17] Boli Zhu, Jingzhong Tong, Jinxun Zhang, et al. Shear properties and design of orthogonal double corrugated plate shear walls [J]. Thin-wall Structures,2023,187:110759.

[18] Fadhil H, Ibrahim I, Mahmood M. Effect of Corrugation Angle and Direction on the Performance of Corrugated Steel Plate Shear Walls[J]. Civil Engineering Journal, 2018,4(11):2667-2679.

[19] Y Boli, Zhu Jingzhong, Tong Jinxun Zhang, et al. Shear properties and Design of orthogonal double corrugated plate shear walls [J]. Thin-wall Structures,2023,187:110759.

[20] Dou C ,Pi Y ,Gao W .Shear resistance and post-buckling behavior of corrugated panels in steel plate shear walls[J].Thin-Walled Structures,2018,131816-826.

[21] Jingzhong Tong, Jinxun Zhang, Wenhua Pan. Ultimate shear resistance and ultimate performance of double corrugated plate shear wall [J]. Journal of Construction Steel Research,2020,165:105895.

[22] Fang J ,Bao W ,Ren F , et al.Experimental study of hysteretic behavior of semi-rigid frame with a corrugated plate[J].Journal of Constructional Steel Research,2020,174.

[23] Yadollahi Y,Pakar I,Bayat M. Performance Evaluation and comparison of corrugated steel plate shear walls [J]. Latin American Journal of Solids and Structures,2015, 12:763-786.

[24] S.M. Ghodratian-Kashan ,S. Maleki .Experimental investigation of double corrugated steel plate shear walls[J].Journal of Constructional Steel Research,2022,190.

[25] S.M. Ghodratian-Kashan ,S. Maleki . Cyclic Performance of Corrugated Steel Plate Shear Walls with Beam-Only-Connected Infill Plates[J]. Advances in Civil Engineering, 2021, 2021(1): 5542613.

[26] S.M. Ghodratian-Kashan ,S. Maleki .Experimental and Numerical Study of Beam-Only-Connected Corrugated Steel Plate Shear Walls[J].Journal of Earthquake Engineering,2024,28(6):1769-1791.